

Second-harmonic response as a tool to detect spin textures in magnetic nodal-line semimetal Fe_3GeTe_2 .

V.D. Esin,¹ A.A. Avakyants,¹ A.V. Timonina,¹ N.N. Kolesnikov,¹ and E.V. Deviatov¹

¹*Institute of Solid State Physics of the Russian Academy of Sciences,
Chernogolovka, Moscow District, 2 Academician Ossipyan str., 142432 Russia*

(Dated: June 28, 2022)

We experimentally investigate second-harmonic transverse voltage response to ac electrical current for a magnetic nodal-line semimetal Fe_3GeTe_2 . For zero magnetic field, the observed response depends as a square of the longitudinal current, as it should be expected for non-linear Hall effect. The magnetic field behavior is found to be sophisticated: while the first-harmonic response shows the known anomalous Hall hysteresis in FGT, the second-harmonic Hall voltage is characterized by the pronounced high-field hysteresis and flat (B -independent) region with curves touching at low fields. The high-field hysteresis strongly depends on the magnetic field sweep rate, so it reflects some slow relaxation process. For the lowest rates, it is also accomplished by multiple crossing points. Similar shape of the second-harmonic hysteresis is known for skyrmion spin textures in non-linear optics. Since skyrmions have been demonstrated for FGT by direct visualization techniques, we can connect the observed high-field relaxation with deformation of the skyrmion lattice. Thus, the second-harmonic Hall voltage response can be regarded as a tool to detect spin textures in transport experiments.

I. INTRODUCTION

Physics of topological semimetals is a new and growing field of modern condensed matter research¹. Dirac semimetals are characterized by gapless spectrum, because of band touching in some distinct points, which are the special points of Brillouin zone. In Weyl semimetals every touching point splits into two Weyl nodes with opposite chiralities due to the time reversal or inversion symmetries breaking. Alternatively, if the band touchings occur along some lines in the three-dimensional Brillouin zone, the material is known as a topological nodal-line semimetal¹⁻⁴. Topologically protected Fermi arc surface states are connecting projections of these nodes on the surface Brillouin zone, which produces complex spin textures⁵⁻⁷ on the surface due to the spin-momentum locking⁸.

One of the promising candidates for magnetic nodal-line semimetal⁹ is a van der Waals ferromagnet Fe_3GeTe_2 (FGT)¹⁰⁻¹⁵. Experimentally, FGT shows large anomalous Hall^{9,16} and Nernst¹⁷ effects, topological Hall effect¹⁸, giant tunneling magnetoresistance¹⁹ and Kondo lattice physics²⁰. Also, the nontrivial topological spin textures - magnetic skyrmions - have been demonstrated^{21,22} in FGT, in addition to the conventional labyrinth domain structure^{23,24}.

FGT magnetization can be investigated by different techniques, but not all of them are sensitive to the relatively small number of spins at the surface of topological semimetals. For example, a typical anomalous Hall hysteresis loop mostly reflects the bulk magnetization behavior²⁵. On the other hand, the harmonic Hall analysis²⁶⁻³² is a known transport technique to study spin textures in different materials. In general, it is a part of a broad approach, which is known also in nonlinear optics³³⁻³⁶, where this technique was demonstrated for optical inves-

tigations of skyrmion structures³⁶.

An important example of the harmonic Hall response in topological materials is the non-linear Hall (NLH) effect³⁷, which is predicted as a transverse current at both zero and twice the frequency³⁸⁻⁵³. NLH effect has been experimentally demonstrated for monolayer transitional metal dichalcogenides^{54,55} and for three-dimensional Weyl and Dirac semimetals^{56,57} as a second-harmonic Hall voltage in zero magnetic field. For FGT, one can also expect that the harmonic Hall analysis in finite magnetic fields can be a powerful tool to investigate spin textures.

Here, we experimentally investigate second-harmonic transverse voltage response to ac electrical current for a magnetic nodal-line semimetal Fe_3GeTe_2 . For zero magnetic field, the observed response depends as a square of the longitudinal current, as it should be expected for non-linear Hall effect. The magnetic field behavior is found to be sophisticated, which we connect with skyrmion spin textures in FGT.

II. SAMPLES AND TECHNIQUE

Fe_3GeTe_2 was synthesized from elements in evacuated silica ampule in a two-step process. At the first step, the load was heated up to 470° C at 10 deg/h rate and the ampule was held at this temperature for 50 h. At the second step, the temperature was increased up to 970° C with the same rate. After 140 h exposure, the ampule was cooled down to the room temperature at 5 deg/h rate. X-ray diffraction data indicates, that the iron tellurides FeTe and FeTe_2 were also found in the material, in addition to the expected Fe_3GeTe_2 compound.

To obtain Fe_3GeTe_2 single crystals, the synthesized mixture was sealed in evacuated silica ampule with some admixture of iodine. The transport reaction was carried

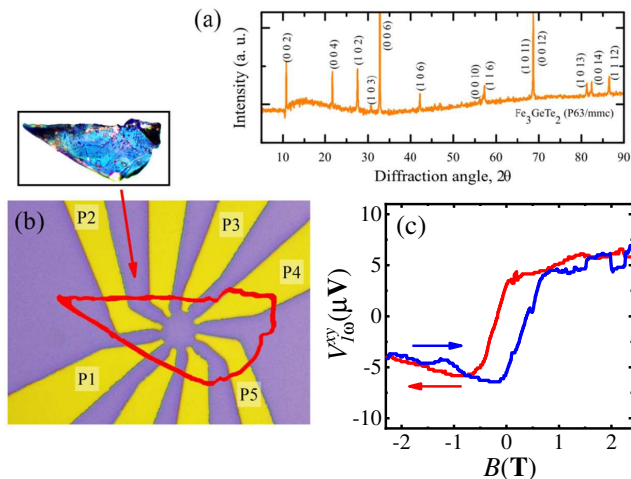


FIG. 1. (Color online) (a) X-ray diffraction pattern (Cu $K\alpha_1$ radiation, $\lambda = 1.540598$ Å), which confirms single-phase Fe_3GeTe_2 with P63/mmc (194) space group ($a = b = 3.991(1)$ Å, $c = 16.33(3)$ Å). (b) Optical image of the Au leads on the insulating SiO_2 substrate. 100 nm thick, $5 \mu\text{m}$ separated leads form a circle in the central part with $18 \mu\text{m}$ diameter. A small (about $100 \mu\text{m}$ size and $0.5 \mu\text{m}$ thick) single-crystal FGT flake is transferred to the leads, as it is depicted by the arrow. The ac current is applied between P1 and P4 contacts, while the transverse (Hall) voltage V^{xy} is measured between the P3 and P5 potential probes. (c) A large anomalous Hall effect as a first-harmonic $V_{1\omega}^{xy}$ hysteresis loop in normal magnetic field, which confirms the known magnetic properties of FGT^{18,63}. The arrows indicate the magnetic field sweep directions.

out for 240 h with temperatures 530°C and 410°C in hot and cold zones, respectively. Afterward, the ampule was quenched in a liquid nitrogen. Water-soluble iron and tellurium iodides were removed in hot distilled water from the obtained Fe_3GeTe_2 single crystals, so the X-ray diffraction analysis confirms single-phase Fe_3GeTe_2 with P63/mmc (194) space group ($a = b = 3.991(1)$ Å, $c = 16.33(3)$ Å), see Fig. 1(a). The known structure model⁵⁸ Fe_3GeTe_2 is refined with single crystal X-ray diffraction measurements (Oxford diffraction Gemini-A, Mo $K\alpha$). The Fe_3GeTe_2 composition is also verified by energy-dispersive X-ray spectroscopy.

Despite FGT is ferromagnetic even for two-dimensional monolayer samples, topological semimetals are essentially three-dimensional objects¹. Thus, we have to select relatively thick (above $0.5 \mu\text{m}$) FGT single crystal flakes, which also ensures sample homogeneity for correct determination of xx- and xy- voltage responses. Thick flakes requires special contact preparation technique: the mechanically exfoliated flake is transferred on the Au leads pattern, which is defined on the standard oxidized silicon substrate by lift-off technique, as depicted in Fig. 1 (b). The transferred flake is shortly pressed to the leads by another oxidized silicon substrate, the latter is removed afterward. This procedure provides transparent FGT-Au junctions (below 1 Ohm resistance), stable in different cooling cycles, which has been verified before for a wide

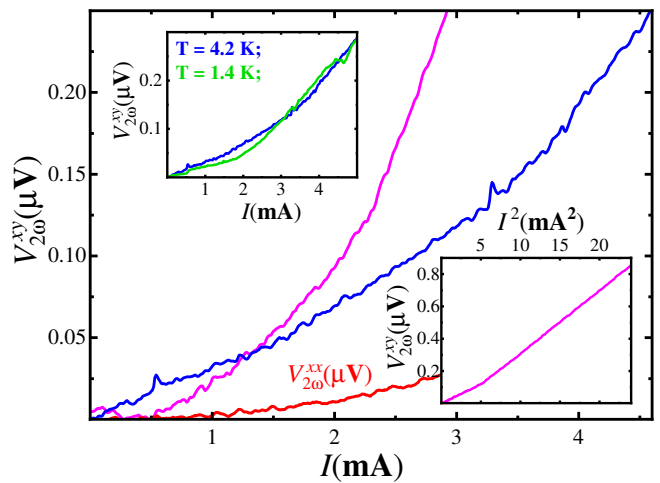


FIG. 2. (Color online) Zero magnetic field. Typical behavior of the transverse second-harmonic voltage component $V_{2\omega}^{xy} \sim I^2$, as it should be expected for the non-linear Hall effect^{54–57}. The longitudinal second-harmonic voltage $V_{2\omega}^{xx}$ is one order of magnitude smaller. The data are presented for two different samples (blue and magenta curves, respectively) at 4.2 K. For clarity, $V_{2\omega}^{xx}$ (red) is only shown for the sample with the highest $V_{2\omega}^{xy}$ values (the magenta curve), the bottom inset demonstrates the square-law $\sim I^2$ dependence for this sample. The upper inset shows $V_{2\omega}^{xy}$ curves for two different temperatures 4.2 and 1.4 K, there is practically no difference in this temperature range.

range of materials^{59–63}. As an additional advantage, the relevant FGT surface with Au contacts (the bottom one) is protected from any contamination by SiO_2 substrate.

We investigate transverse (xy-) first- and second-harmonic voltage responses by standard four-point lock-in technique. The ac current is applied between P1 and P4 contacts in Fig. 1 (b), while the transverse (Hall) voltage V^{xy} is measured between the P3 and P5 potential probes. Also, the longitudinal V^{xx} component can be measured between the P2 and P3. The Curie temperature of bulk FGT crystals¹⁸ is about ≈ 220 K, so the measurements are performed at the liquid helium temperatures. Similar results are obtained for several samples in different cooling cycles.

III. EXPERIMENTAL RESULTS

We confirm the correctness of the experimental conditions by demonstrating first-harmonic $V_{1\omega}^{xy}$ anomalous Hall hysteresis loop, see Fig. 1 (c). A large anomalous Hall effect manifests itself as non-zero Hall voltage in zero magnetic field, which is determined by the bulk magnetization direction. The observed first-harmonic hysteresis loop well corresponds to the known anomalous Hall effect in FGT^{18,63}.

In zero external magnetic field, Fig. 2 shows typical behavior of the non-linear Hall effect^{54–57} as a quadratic transverse Hall-like response $V_{2\omega}^{xy}$ to ac excitation current

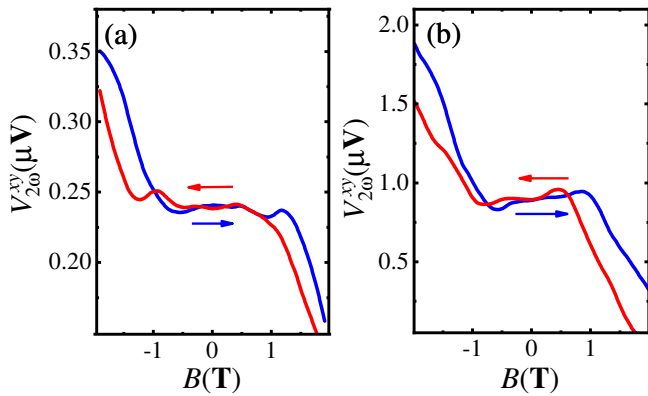


FIG. 3. (Color online) Asymmetric $V_{2\omega}^{xy}(B)$ magnetic field dependence, which is qualitatively similar for two different samples with strongly different $V_{2\omega}^{xy}$ values ((a) and (b), respectively, for the fixed ac current $I = 4.5$ mA). The expected linear $\sim B$ field contribution is accomplished by pronounced high-field hysteresis and flat (B -independent) region with curves touching at low fields, within ± 1 T. The hysteresis is defined by magnetic field sweep direction, as indicated by arrows of the same color. The curves are shown for high, 8 mT/s sweep rate for normal orientation of the magnetic field, at 4.2 K temperature.

I for two different samples. The $\sim I^2$ dependence is directly demonstrated in the bottom inset to Fig. 2. The longitudinal second-harmonic voltage $V_{2\omega}^{xx}$ is one order of magnitude smaller, which confirms well-defined Au leads geometry and a homogeneous FGT flake. There is no noticeable temperature dependence in the 1.4-4.2 K range, see the upper inset in Fig. 2, since the FGT spectrum is well-established much below the ≈ 220 K Curie temperature¹⁸. Thus, we observe non-linear Hall effect for magnetic nodal-line semimetal FGT.

In the magnetic field, Fig. 3 shows asymmetric $V_{2\omega}^{xy}(B)$ dependences for two opposite field sweep directions. The linear $\sim B$ field contribution can be expected^{68,69} for the NLH effect signal, which is an origin of $V_{2\omega}^{xy}(B)$ asymmetry, as it was experimentally confirmed for non-magnetic topological semimetals⁵⁶. However, Fig. 3 shows much more sophisticated behavior for ferromagnetic FGT flakes. We indeed observe linear field dependence in high magnetic fields, which is accomplished by pronounced hysteresis and flat (B -independent) region with curves touching at low fields, within ± 1 T. This $V_{2\omega}^{xy}(B)$ behavior is qualitatively similar for two different samples with strongly different $V_{2\omega}^{xy}$ values in Fig. 3 (a) and (b).

The hysteresis amplitude depends on the magnetic field sweep rate, while the hysteresis itself is present even for the lowest rates, see Fig. 4. We observe pronounced hysteresis in the $V_{2\omega}^{xy}(B)$ curves with the magnetic field sweep direction for high, 8 mT/s sweep rate in Fig. 3, while it is much smaller for 1 mT/s in Fig. 4, so the high-field hysteresis reflects some slow relaxation process. At the lowest sweep rates, multiple crossing points are

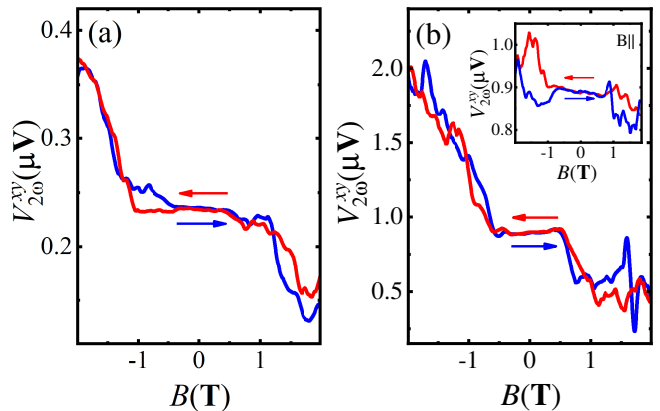


FIG. 4. (Color online) $V_{2\omega}^{xy}(B)$ curves for the lowest, for 1 mT/s sweep rate, (a) and (b) panels are for two samples from Fig. 3, respectively. The hysteresis amplitude is significantly smaller in this case, there are multiple crossing points for the curves, which usually reflects some inhomogeneous magnetization process³⁴⁻³⁶, so the details of the hysteresis loops differ for two samples. The curves are obtained at 4.2 K for normal orientation of the magnetic field and the fixed ac current $I = 4.5$ mA. Inset shows much more pronounced hysteresis for the in-plane magnetic field orientation for the same (1 mT/s) sweep rate, while the magnetic field dependence itself is weaker in this case. Arrows indicate the magnetic field sweep direction.

also observed, so the details of the hysteresis loop differ for two samples in Fig. 4 (a) and (b). Multiple crossing points usually reflect inhomogeneous magnetization process for spin textures in the sample³⁴⁻³⁶. Inset to Fig. 4 shows non-linear planar Hall effect⁶⁴ as the asymmetric $V_{2\omega}^{xy}(B)$ behavior for the in-plane magnetic field orientation. Despite the results are qualitatively similar for two field orientations, the hysteresis is more pronounced in the parallel field even for the lowest (1 mT/s) sweep rate, while the magnetic field dependence itself is weaker for the parallel field.

IV. DISCUSSION

As a result, while the NLH effect could be expected for Fe_3GeTe_2 in zero magnetic field, the sophisticated behavior of $V_{2\omega}^{xy}(B)$ requires consistent explanation.

In principle, second-harmonic hysteresis could also arise from Joule heating $\sim RI^2$ of the sample with low thermoconductance²⁸. On the other hand, sample magnetoresistance $R(B)$ is not sensitive to the magnetic field sign, so any thermoelectric effects should be symmetric in magnetic field^{28,56,65,66}, in contrast to experimental asymmetric (odd) magnetic field dependences in Fig. 3. The hysteresis can not also originate from the experimental equipment, since we never observed $V_{2\omega}^{xy}(B)$ hysteresis for non-magnetic samples in similar experiments^{56,66}.

The hysteresis in Hall voltage $V_{1\omega}^{xy}$ is known for FGT flakes in the external magnetic field^{18,63} as anomalous

Hall effect¹. For topological materials, it is usually regarded as the indication of a magnetic topological phase, as supported, e.g., by the topological-insulator-multilayer model, so the one-dimensional Chern edge states form the two-dimensional surface states¹. Irrespective of the particular mechanism, anomalous Hall effect reflects the bulk magnetization of the ferromagnetic FGT flakes^{18,63}: $V_{1\omega}^{xy}$ Hall voltage changes its sign if the bulk magnetization is reversed by the external magnetic field. Experimentally, the Hall voltage hysteresis well corresponds to the $M(H)$ magnetization reversal curves, see, e.g., Ref.²⁵.

These considerations can not be directly applied to the second-harmonic Hall voltage component, since the non-linear Hall effect arises from the Berry curvature in momentum space³⁷. In the simplified picture, an a.c. excitation current generates the effective sample magnetization, which leads to the Hall effect even in zero external magnetic field. Hall voltage is therefore proportional to the square of the excitation current, so it can be detected as the second-harmonic transverse voltage component $V_{2\omega}^{xy}$, as we observe in Fig. 2. Another possible contribution to the non-linear Hall effect is skew scattering with nonmagnetic impurities in time-reversal-invariant noncentrosymmetric materials⁶⁷, but it hardly be applied to the ferromagnetic FGT semimetal.

Theoretically predicted $V_{2\omega}^{xy}$ sensitivity to the external magnetic field^{68,69} indicates, that $V_{2\omega}^{xy}$ should also be sensitive to the internal bulk FGT magnetization. From the comparison of Figs. 1 (c) and 3, the internal magnetization is dominant within ± 1 T, the region of the $V_{1\omega}^{xy}$ hysteresis loop, while the linear $V_{2\omega}^{xy}(B) \sim B$ dependence on the external field appears beyond this region in Fig. 3. This well describes the flat region in the experimental $V_{2\omega}^{xy}(B)$ curves, but the high-field hysteresis seems to have a different origin, because the internal magnetization is not sensitive to the magnetic field outside ± 1 T, see Fig. 1 (c). On the other hand, similar hysteresis is known for nonlinear optics, where a second-harmonic signal is a powerful method to analyze skyrmion spin textures in magnetic materials³⁴⁻³⁶. For the FGT semimetal, a high-density lattice of hexagonally packed skyrmions can be induced by a simple cooling process^{21,22}. By Bitter decoration technique^{70,71}, we also confirmed the labyrinth domain structure^{23,24} for our FGT samples, as well as the hexagonally packed skyrmions²².

Deformation of the skyrmion lattice can be responsible for the observed hysteresis with the magnetic field sweep direction. Indeed, skyrmions appear in magnetic materials due to the Dzyaloshinsky-Moriya interaction⁷². The competition between the perpendicular magnetic anisotropy and magnetic dipole-dipole interaction is crucial for skyrmions, so the spin textures should be sensitive to the external magnetic field. This conclusion

is strongly confirmed by the $V_{2\omega}^{xy}(B)$ dependence on the field sweep rate in Figs. 3 and 4. At the lowest rate, multiple crossing points are observed in a good correspondence with the known behavior for skyrmion spin textures in optics, where multiple crossing points reflect inhomogeneous magnetization in the presence of skyrmion structures³⁴⁻³⁶. The particular skyrmion distribution is obviously different for different samples, so the details of the shape of the hysteresis loop differs in Fig. 4 (a) and (b). On the other hand, the curves are very similar for high sweep rates, where the hysteresis only reflects the deformation of the skyrmion lattice.

For the in-plane magnetic field, one can also expect B -like correction to the $V_{2\omega}^{xy}(B)$ dependence^{69,73}. The surface spin textures should be sensitive to the direction of the external magnetic field, so the slow relaxation is more pronounced in the inset to Fig. 4, while the flat region is approximately of the same width for the experimental $V_{2\omega}^{xy}(B)$ curves. This confirms our interpretation, so the second-harmonic Hall response $V_{2\omega}^{xy}(B)$ is a powerful tool to detect spin textures in magnetic nodal-line semimetals.

V. CONCLUSION

As a conclusion, we observe sophisticated magnetic field behavior of the second-harmonic Hall voltage response: while the first-harmonic signal shows the known anomalous Hall hysteresis in FGT, the second-harmonic Hall voltage is characterized by the pronounced high-field hysteresis and flat (B -independent) region in $V_{2\omega}^{xy}(B)$ with curves touching at low fields. The high-field hysteresis reflects some slow relaxation process, so it strongly depends on the magnetic field sweep rate. For the lowest rates, it is also accomplished by multiple crossing points. The low-field curves touching and the shape of the second-harmonic hysteresis with multiple crossing points are known for skyrmion spin textures in nonlinear optics. Since skyrmions have been demonstrated for FGT by direct visualization techniques, we can connect the observed high-field relaxation with deformation of the skyrmion lattice. This conclusion is confirmed by the $V_{2\omega}^{xy}(B)$ sensitivity to the direction of the external magnetic field, as it should be expected for surface spin textures. Thus, the second-harmonic Hall response hysteresis can be regarded as the manifestation of Fe_3GeTe_2 skyrmion structures in transport experiments.

ACKNOWLEDGMENTS

We wish to thank S.S Khasanov for X-ray sample characterization. We gratefully acknowledge financial support by the RF State task.

- ¹ As a recent review see N.P. Armitage, E.J. Mele, and A. Vishwanath, *Rev. Mod. Phys.* 90, 015001 (2018).
- ² Fang, C., L. Lu, J. Liu, and L. Fu, 2016, *Nature Physics* 12(10), 936.
- ³ B. Bradlyn, J. Cano, Z. Wang, M. G. Vergniory, C. Felser, R. J. Cava, and B. A. Bernevig, *Science* 353, aaf5037 (2016)
- ⁴ Peizhe Tang, Quan Zhou, and Shou-Cheng Zhang, *Phys. Rev. Lett.* 119, 206402 (2017)
- ⁵ J. Jiang, F. Tang, X.C. Pan, H.M. Liu, X.H. Niu, Y.X. Wang, D.F. Xu, H.F. Yang, B.P. Xie, F.Q. Song, P. Dudin, T.K. Kim, M. Hoesch, P.K. Das, I. Vobornik, X.G. Wan, and D.L. Feng, *Phys. Rev. Lett.* 115, 166601 (2015).
- ⁶ D. Rhodes, S. Das, Q.R. Zhang, B. Zeng, N.R. Pradhan, N. Kikugawa, E. Manousakis, and L. Balicas, *Phys. Rev. B* 92, 125152 (2015).
- ⁷ Y. Wang, K. Wang, J. Reutt-Robey, J. Paglione, and M. S. Fuhrer, *Phys. Rev. B* 93, 121108 (2016).
- ⁸ Su-Yang Xu, Chang Liu, Satya K. Kushwaha, Raman Sankar, Jason W. Krizan, Ilya Belopolski, Madhab Neupane, Guang Bian, Nasser Alidoust, Tay-Rong Chang, Horng-Tay Jeng, Cheng-Yi Huang, Wei-Feng Tsai, Hsin Lin, Pavel P. Shibayev, Fang-Cheng Chou, Robert J. Cava, and M. Zahid Hasan, *Science*, 347 (6219), DOI: 10.1126/science.1256742.
- ⁹ K. Kim, J. Seo, E. Lee, K.-T. Ko, B. S. Kim, Bo G. Jang, J. M. Ok, J. Lee, Y. J. Jo, W. Kang, J. H. Shim, C. Kim, H. W. Yeom, B. I. Min, B.-J. Yang, and J. S. Kim, *Nat. Mater.* 17, 794 (2018).
- ¹⁰ Y. Deng, Y. Yu, Y. Song, J. Zhang, N. Z. Wang, Z. Sun, Y. Yi, Y. Z. Wu, S. Wu, J. Zhu, J. Wang, X. H. Chen, and Y. Zhang, *Nature* 563, 94 (2018). <https://doi.org/10.1038/s41586-018-0626-9>
- ¹¹ J.-J. Guo, Q.-L. Xia, X.-G. Wang, Y.-Z. Nie, R. Xiong, G.-H. Guo, *J. Magn. Magn. Mater.* 527, 167719 (2021). doi: 10.1016/j.jmmm.2020.167719
- ¹² C. Tan, J. Lee, S. G. Jung, T. Park, S. Albarakati, J. Partridge, M. R. Field, D. G. McCulloch, L. Wang, and C. Lee, *Nat. Commun.* 9, 1554 (2018). <https://doi.org/10.1038/s41467-018-04018-w>
- ¹³ H. L. Zhuang, P. R. C. Kent, R. G. Henning, *Phys. Rev. B*. 93, 134407 (2016).
- ¹⁴ L. Cai, C. Yu, L. Liu, W. Xia, H.-A. Zhou, L. Zhao, Y. Dong, T. Xu, Z. Wang, Y. Guo, Y. Zhao, J. Zhang, L. Yang, L. Yang, and W. Jiang, *Appl. Phys. Lett.* 117, 192401 (2020). <https://doi.org/10.1063/5.0030607>
- ¹⁵ B. Chen, J. H. Yang, H. D. Wang, M. Imai, H. Ohta, C. Michioka, K. Yoshimura, and M. H. Fang, *J. Phys. Soc. Jpn.* 82, 124711 (2013).
- ¹⁶ Y. Wang, C. Xian, J. Wang, B. Liu, L. Ling, L. Zhang, L. Cao, Z. Qu, and Y. Xiong, *Phys. Rev. B*. 96, 134428 (2017).
- ¹⁷ J. Xu, W. A. Phelan, C.-L. Chien, *Nano Lett.*, 19, 8250 (2019).
- ¹⁸ Y. You, Y. Gong, H. Li, Z. Li, M. Zhu, J. Tang, E. Liu, Y. Yao, G. Xu, F. Xu, and W. Wang, *Phys. Rev. B* 100, 134441 (2019).
- ¹⁹ T. Song, X. Cai, M. W.-Y. Tu, X. Zhang, B. Huang, N. P. Wilson, K. L. Seyler, L. Zhu, T. Taniguchi, K. Watanabe, M. A. McGuire, D. H. Cobden, D. Xiao, W. Yao, X. Xu., *Science* 360, 1214–1218 (2018).
- ²⁰ Y. Zhang, H. Lu, X. Zhu, S. Tan, W. Feng, Q. Liu, W. Zhang, Q. Chen, Y. Liu, X. Luo, D. Xie, L. Luo, Z. Zhang, and X. Lai, *Sci. Adv.* 4, eaao6791 (2018). <https://doi.org/10.1126/sciadv.aao6791>
- ²¹ M. Yang, Q. Li, R. V. Chopdekar, R. Dhall, J. Turner, J. D. Carlström, C. Ophus, C. Klewe, P. Shafer, A. T. N'Diaye, J. W. Choi, G. Chen, Y. Z. Wu, C. Hwang, F. Wang, and Z. Q. Qiu, *Sci Adv.* 6(36): eabb5157. (2020)
- ²² Bei Ding, Zefang Li, Guizhou Xu, Hang Li, Zhipeng Hou, Enke Liu, Xuekui Xi, Feng Xu, Yuan Yao, and Wenhong Wang, *Nano Lett.*, 20, 2, 868–873 (2020)
- ²³ Giang D. Nguyen, Jinhwan Lee, Tom Berlijn, Qiang Zou, Saban M. Hus, Jewook Park, Zheng Gai, Changgu Lee, and An-Ping Li, *Phys. Rev. B* 97, 014425 (2018)
- ²⁴ Qian Li, Mengmeng Yang, Cheng Gong, Rajesh V. Chopdekar, Alpha T. N'Diaye, John Turner, Gong Chen, Andreas Scholl, Padraic Shafer, Elke Arenholz, Andreas K. Schmid, Sheng Wang, Kai Liu, Nan Gao, Alemayehu S. Admasu, Sang-Wook Cheong, Chanyong Hwang, Jia Li, Feng Wang, Xiang Zhang, and Ziqiang Qiu, *Nano Lett.*, 18, 9, 5974–5980 (2018)
- ²⁵ Ella Lachman, Ryan A. Murphy, Nikola Maksimovic, Robert Kealhofer, Shannon Haley, Ross D. McDonald, Jeffrey R. Long and James G. Analytis, *Nature Communications*, 11, 560 (2020).
- ²⁶ M. Hayashi, J. Kim, M. Yamanouchi, and H. Ohno, *Physical Review B* 89, 144425 (2014).
- ²⁷ N. Vlietstra, J. Shan, B. Van Wees, M. Isasa, F. Casanova, and J. B. Youssef, *Physical Review B* 90, 174436 (2014).
- ²⁸ C. O. Avci, K. Garelo, M. Gabureac, A. Ghosh, A. Fuhrer, S. F. Alvarado, and P. Gambardella, *Physical Review B* 90, 224427 (2014).
- ²⁹ D. MacNeill, G. M. Stiehl, M. H. Guimaraes, N. D. Reynolds, R. A. Buhrman, and D. C. Ralph, *Physical Review B* 96, 054450 (2017).
- ³⁰ Y. Chen, D. Roy, E. Cogulu, H. Chang, M. Wu, and A. D. Kent, *Applied Physics Letters* 113, 202403 (2018).
- ³¹ C. F. Schippers, H. J. Swagten, and M. H. Guimarães, *Physical Review Materials* 4, 084007 (2020).
- ³² F. Feringa, G. E. W. Bauer, B. J. van Wees, [arXiv:2201.13241](https://arxiv.org/abs/2201.13241)
- ³³ Manfred Fiebig, Victor V. Pavlov, and Roman V. Pisarev., *Journal of the Optical Society of America B* Vol. 22, Issue 1, pp. 96-118 (2005)
- ³⁴ T.V. Murzina, K.A. Lazareva, E.E. Shalygina, I.A. Kolmychek, E.A. Karashtin, N.S. Gusev, A.A. Fraerman., <https://arxiv.org/abs/1812.03922>
- ³⁵ V. L. Krutyanskiy, I. A. Kolmychek, B. A. Gribkov, E. A. Karashtin, E. V. Skorohodov, and T. V. Murzina., *Phys. Rev. B* 88, 094424 (2013)
- ³⁶ Roméo Juge, Naveen Sisodia, Joseba Urrestarazu Larrañaga, Qiang Zhang, Van Tuong Pham, Kumari Gaurav Rana, Brice Sarpi, Nicolas Mille, Stefan Stanescu, Rachid Belkhou, Mohamad-Assaad Mawass, Nina Novakovic-Marinkovic, Florian Kronast, Markus Weigand, Joachim Gräfe, Sebastian Wintz, Simone Finizio, Jörg Raabe, Lucia Aballe, Michael Foerster, Mohamed Belmeguenai, Liliana Buda-Prejbeanu, Justin M. Shaw, Hans T. Nembach, Laurent Ranno, Gilles Gaudin, Olivier Boulle., <https://arxiv.org/abs/2111.11878>

- ³⁷ Inti Sodemann, Liang Fu., Phys. Rev. Lett. 115, 216806 (2015)
- ³⁸ E. Deyo, L. E. Golub, E. L. Ivchenko, and B. Spivak, arXiv:0904.1917 (2009).
- ³⁹ L.E. Golub, E.L. Ivchenko, B.Z. Spivak, JETP Letters, 105, 782 (2017)
- ⁴⁰ J. E. Moore and J. Orenstein, Phys. Rev. Lett., 105, 026805 (2010).
- ⁴¹ T. Low, Y. Jiang, and F. Guinea, Physical Review B 92, 235447 (2015).
- ⁴² Y. Zhang, J. van den Brink, C. Felser, and B. Yan, 2D Materials 5, 044001 (2018).
- ⁴³ Z. Z. Du, C. M. Wang, H.-Z. Lu, and X. C. Xie, Phys. Rev. Lett. 121, 266601 (2018).
- ⁴⁴ Z. Z. Du, C. M. Wang, S. Li, H.-Z. Lu, and X. C. Xie, Nature Commun. 10, 3047 (2019).
- ⁴⁵ C. Xiao, Z. Z. Du, and Q. Niu, Phys. Rev. B 100, 165422 (2019).
- ⁴⁶ S. Nandy and I. Sodemann, Phys. Rev. B 100, 195117 (2019).
- ⁴⁷ H. Wang and X. Qian, npj Comput. Mater. 5, 1 (2019).
- ⁴⁸ B. T. Zhou, C.-P. Zhang, and K. T. Law, Phys. Rev. Applied 13, 024053 (2020).
- ⁴⁹ H. Rostami and V. Juričić, Phys. Rev. Research 2, 013069 (2020).
- ⁵⁰ D.-F. Shao, S.-H. Zhang, G. Gurung, W. Yang, and E. Y. Tsybmal, Phys. Rev. Lett. 124, 067203 (2020).
- ⁵¹ S. Singh, J. Kim, K. M. Rabe, and D. Vanderbilt, Phys. Rev. Lett. 125, 046402 (2020) 10.1103/PhysRevLett.125.046402
- ⁵² M. W.-Y. Tu, C. Li, H. Yu, and W. Yao, 2D Mater. (2020) 10.1088/2053-1583/ab89e8
- ⁵³ Z. Z. Du, C. M. Wang, Hai-Peng Sun, Hai-Zhou Lu, X. C. Xie, arXiv:2004.09742 (2020)
- ⁵⁴ Qiong Ma, Su-Yang Xu, Huitao Shen, David MacNeill, Valla Fatemi, Tay-Rong Chang, Andrés M. Mier Valdivia, Sanfeng Wu, Zongzheng Du, Chuang-Han Hsu, Shiang Fang, Quinn D. Gibson, Kenji Watanabe, Takashi Taniguchi, Robert J. Cava, Efthimios Kaxiras, Hai-Zhou Lu, Hsin Lin, Liang Fu, Nuh Gedik and Pablo Jarillo-Herrero., Nature 565, 337 (2019).
- ⁵⁵ K. Kang, T. Li, E. Sohn, J. Shan, and K. F. Mak, Nature Mater. 18, 324 (2019).
- ⁵⁶ O. O. Shvetsov, V. D. Esin, A. V. Timonina, N. N. Kolesnikov, and E. V. Deviatov, JETP Letters, 109, 715–721 (2019). DOI: 10.1134/S0021364019110018
- ⁵⁷ A. Tiwari, F. Chen, Sh. Zhong, E. Druke, J. Koo, A. Kaczmarek, C. Xiao, J. Gao, X. Luo, Q. Niu, Y. Sun, B. Yan, L. Zhao and A. W. Tseng, Nat. Commun. 12, 2049 (2021). <https://doi.org/10.1038/s41467-021-22343-5>
- ⁵⁸ H.-J. Deiseroth, K. Aleksandrov, C. Reiner, L. Kienle, and R. K. Kremer, Eur. J. Inorg. Chem. 2006, 1561
- ⁵⁹ O. O. Shvetsov, V. D. Esin, A. V. Timonina, N. N. Kolesnikov, and E. V. Deviatov Phys. Rev. B 99, 125305 (2019)
- ⁶⁰ O. O. Shvetsov, V. D. Esin, A. V. Timonina, N. N. Kolesnikov, E. V. Deviatov EPL, 127, 57002 (2019)
- ⁶¹ N. N. Orlova, N. S. Ryshkov, A. A. Zagitova, V. I. Kulakov, A. V. Timonina, D. N. Borisenko, N. N. Kolesnikov, and E. V. Deviatov Phys. Rev. B 101, 235316 (2020)
- ⁶² V. D. Esin, D. N. Borisenko, A. V. Timonina, N. N. Kolesnikov, and E. V. Deviatov Phys. Rev. B 101, 155309 (2020)
- ⁶³ O. O. Shvetsov, Yu. S. Barash, A. V. Timonina, N. N. Kolesnikov, E. V. Deviatov, JETP Letters, 115, 267–275 (2022). DOI: 10.1134/S0021364022100101
- ⁶⁴ Pan He, Steven S.-L. Zhang, Dapeng Zhu, Shuyuan Shi, Olle G. Heinonen, Giovanni Vignale, and Hyunsoo Yang Phys. Rev. Lett. 123, 016801 (2019)
- ⁶⁵ N. Vlietstra, J. Shan, B. J. van Wees, M. Isasa, F. Casanova, and J. Ben Youssef Phys. Rev. B 90, 174436 (2014)
- ⁶⁶ V. D. Esin, A. V. Timonina, N. N. Kolesnikov, and E. V. Deviatov, JETP Letters volume 111, pages685–689 (2020).
- ⁶⁷ Hiroki Isobe, Su-Yang Xu, Liang Fu, Sci. Adv. 6, eaay2497 (2020) doi: 10.1126/sciadv.aay2497
- ⁶⁸ Debottam Mandal, Kamal Das, Amit Agarwal, arXiv:2201.02505
- ⁶⁹ A. A. Zyuzin and A. Yu. Zyuzin, Phys. Rev. B 95, 085127 (2017). DOI: 10.1103/PhysRevB.95.085127
- ⁷⁰ I. V. Grigorieva, W. Escoffier, J. Richardson, L. Y. Vinnikov, S. Dubonos, and V. Oboznov., PRL. 96, 077005 (2006)
- ⁷¹ M. R. Eskildsen, L. Ya. Vinnikov, T. D. Blasius, I. S. Veshchunov, T. M. Artemova, J. M. Densmore, C. D. Dewhurst, N. Ni, A. Kreyssig, S. L. Bud'ko, P. C. Canfield, and A. I. Goldman., PRB 79, 100501(R) (2009)
- ⁷² I. Dzyaloshinskii (1958). Journal of Physics and Chemistry of Solids. 4 (4): 241. doi:10.1016/0022-3697(58)90076-3
- ⁷³ Rui-Hao Li, Olle G. Heinonen, Anton A. Burkov, and Steven S.-L. Zhang, Phys. Rev. B 103, 045105 (2021)